Lawrence Berkeley National Laboratory

Lawrence Berkeley National Laboratory

Title

Resonant x-ray emission spectroscopy of liquid water: novel instrumentation, high resolution, and the "map" approach

Permalink

https://escholarship.org/uc/item/5s8762c3

Author

Weinhardt, L.

Publication Date

2009-03-13

Peer reviewed

eScholarship.org Powered by the California Digital Library
University of California

Resonant x-ray emission spectroscopy of liquid water: novel instrumentation, high resolution, and the "map" approach

L. Weinhardt[1,*], O. Fuchs[2], M. Blum[2], M. Bär[1], M. Weigand[2], J.D. Denlinger[3], Y. Zubavichus[4], M. Zharnikov[4], M. Grunze[4], C. Heske[1,*], and E. Umbach[2]

[1]*Department of Chemistry, University of Nevada, Las Vegas, NV 89154-4003, USA*

[2]*Universität Würzburg, Experimentelle Physik II, Am Hubland, 97074 Würzburg, Germany*

[3]*Advanced Light Source, Lawrence Berkeley National Laboratory, 1 Cyclotron Road, Berkeley, CA 94720, USA*

[4]*Angewandte Physikalische Chemie, Universität Heidelberg, INF 253, 69120 Heidelberg, Germany*

* To whom correspondence should be addressed: lothar.weinhardt@physik.uni-wuerzburg.de (L.Weinhardt) and heske@unlv.nevada.edu (C. Heske)

Abstract:

Techniques to study the electronic structure of liquids are rare. Most recently, resonant x-ray emission spectroscopy (XES) has been shown to be an extremely versatile spectroscopy to study both occupied and unoccupied electronic states for liquids in thermodynamic equilibrium. However, XES requires high-brilliance soft x-ray synchrotron radiation and poses significant technical challenges to maintain a liquid sample in an ultra-high vacuum environment. Our group has therefore developed and constructed a novel experimental setup for the study of liquids, with the long-term goal of investigating the electronic structure of biological systems in aqueous environments. We have developed a flow-through liquid cell in which the liquid is separated from vacuum by a thin Si_3N_4 or SiC window and which allows a precise control of temperature. This approach has significant advantages compared to static liquids cells used in the past. Furthermore, we have designed a dedicated high-transmission, high-resolution soft x-ray spectrometer. The high transmission makes it possible to measure complete resonant XES "maps" in less than an hour, giving unprecedented detailed insight into the electronic structure of the investigated sample. Using this new equipment we have investigated the electronic structure of liquid water. Furthermore, our XES spectra and maps give information about ultra-fast dissociation on the timescale of the O 1s core hole lifetime, which is strongly affected by the initial state hydrogen bonding configuration.

Introduction

Despite extensive experimental and theoretical efforts [1-10], the local hydrogen bridge bond configuration ("structure") of liquid water is still under debate [1-3,10,11]. In the liquid state, hydrogen bonds (HBs) between the individual water molecules are formed and broken dynamically. Time averaged geometrical information has been available through neutron and x-ray scattering and infrared spectroscopy (see, e.g. [1,12]). More recently, synchrotron-based techniques which probe the electronic structure, namely photoelectron spectroscopy (PES), x-ray absorption spectroscopy (XAS), and (resonant) x-ray emission spectroscopy (XES) have been applied to liquid water and ice. While PES requires a water jet injected into the vacuum chamber and therefore is probing the system in a thermodynamic non-equilibrium state (see also below), XAS and XES can be performed on liquids under ambient conditions (i.e., near atmospheric pressure).

XAS gives local, partial information about the unoccupied states of the investigated samples. It is "local" in the sense that it probes only unoccupied states that have a significant wave function overlap with the excited core level (in the case of water: O 1s). "Partial" refers to the fact that the XAS process is (in first approximation) a dipole transition with corresponding selection rules, which gives information about the symmetry of the involved orbitals. For XAS of water, absorption resonances related to the unoccupied $4a_1$ and $2b_2$ orbitals are observed, with the pre- and post-edge regions considered as signatures for distorted and fully coordinated HB configurations of water molecules, respectively [1,4,6,9]. The interpretation of the spectra is quite difficult and relies mostly on molecular dynamics (MD) simulations and first-principle calculations [1,2,4,6,8,10,13].

In the resonant XES process both, unoccupied states and valence states are involved. Similar to XAS, XES is also a partial local probe. When using it non-resonantly (i.e., with an excitation energy high above the absorption threshold), the wave function overlap between the core hole (in our case O 1s) and the valence orbital as well as symmetry and dipole selection rules determine the intensity of the respective transition. When using resonant excitation, selection rules and selective excitations give additional insight into the occupied *and* unoccupied electronic structure of the system. In XES of water, three emission peaks related to the occupied $1b_2$, $3a_1$, and $1b_1$ orbitals are observed for the liquid state [14-16], for gas phase water [17], and for ice [18]. High-resolution XES (HRXES) spectra of ice reveal a clear splitting of the $1b_1$ orbital [18], whereas the HRXES spectrum of gas phase water is dominated by a single $1b_1$ peak [17]. First investigations of liquid water using XES only showed one broad $1b_1$ peak [9,14], but new HRXES spectra clearly show a splitting [19,20], as will be discussed below. In addition, we observe a strong isotope effect and a weak temperature dependence. As will be discussed below, these observations can be explained by ultra-fast dissociation of the water molecule during the XES process, which is influenced by its hydrogen bonding environment.

In the following, we will first describe our flow-through liquid cell setup used for the experiments, then discuss our high-resolution, high-transmission x-ray spectrometer and its capability to measure entire resonant x-ray emission "maps", and finally discuss selected results for water and heavy water.

The flow-through liquid cell

Investigating liquids with soft x-rays is a challenging task. The high excitation photon flux needed for such experiments requires the use of high-brilliance soft x-rays from a third-generation synchrotron source and hence the experiments, in principle, have to be performed in an ultra-high vacuum environment. One approach is to use electron- or ion-yield x-ray absorption (XAS) or photoelectron spectroscopy (PES) on a liquid micro jet, injected directly into the vacuum chamber [7,8]. Apart from the technical difficulties to maintain the analysis chamber and the beamline at a low enough pressure, the liquid in such a jet is not in thermodynamic equilibrium, which complicates the interpretation of the data, especially in the case of solutions. In addition, a considerable contribution of signal from vapor surrounding the jet compromises the results.

For XES and XAS (using fluorescence yield detection) a different approach can be used. Due to the photon-in/photon-out nature of these techniques the inelastic mean free path is long enough that a thin window membrane can be used to separate the vacuum from the probed liquid at atmospheric pressure. Several investigations of liquids using this concept can be found in the literature [9,14,21,22]. In these publications, a "static" liquid cell setup was used, which consists of a droplet of the investigated liquid sealed behind a window membrane.

There are several disadvantages of this approach. The temperature of the investigated liquid can not be controlled accurately, since high x-ray intensity may lead to a strong local temperature rise close to the membrane and, even worse, to decomposition of the investigated liquid. The latter may include the formation of gas bubbles and the accumulation of fragments in the liquid and on the window membrane. Furthermore, the cell needs to be transferred out of the vacuum chamber

and, in some designs, the window membrane needs to be removed every time the liquid is exchanged.

Based on our experience with static liquid cells, we have developed a flow-through liquid cell (note that a similar set-up was developed by Guo et al. [23]). In this design, we continuously pump the liquid via stainless steel tubing through the probing volume (see Fig. 1), enabling us to easily change liquids, reliably control their temperature within ±0.1°K, as well as control and avoid beam damage contributions in our spectra. It also reliably avoids gas bubble formation up to the boiling temperature of the liquid. The cell body is made of Teflon and features an integrated thermocouple that allows monitoring the temperature of the liquid in the probing volume. We have used Si_3N_4 as well as SiC window membranes with a thickness of 100 nm. A detailed description of our setup can be found in [24].

A novel high-resolution, high-transmission x-ray spectrometer

For the study of biologically relevant solutions, we have developed a variable line spacing (VLS) spectrometer optimized for the photon energy range between 130 eV and 650 eV. A detailed description of the spectrometer can be found in [25]. Its slit-less design (shown in Fig. 2) consists of a spherical mirror "M" combined with the VLS grating "G". This combination was originally proposed by Hettrick and Underwood [26]. The VLS grating is designed such that the entire energy range is covered by making use of higher diffraction orders for higher energies. A CCD detector is used in normal incidence, which is its most efficient geometry. To mask parts of the mirror, an adjustable aperture A can be used, but since the resolving power of the spectrometer ($E/\Delta E>1200$ over the whole energy range) is not limited by imaging aberrations, this is only done

for calibration purposes. The spectrometer is designed such that (despite its slit-less design) a spot size of 30 microns in the dispersive direction is sufficient to achieve the resolving power of the spectrometer. This moderate spot size reduces the requirements for the beamline and minimizes beam damage effects.

While a variety of different new designs have been developed over the last few years [27-31], our VLS spectrometer exhibits a significantly higher transmission than current state-of-the-art spectrometers. A direct comparison with the permanently installed "SXF" spectrometer at Beamline 8.0 of the Advanced Light Source (ALS) [31] (note that this is an outstanding spectrometer with comparable spectral resolution, e.g., at the oxygen K edge [19]) showed an efficiency gain of about two orders of magnitude over the whole photon energy range. With this huge gain we are now able to change the way a resonant x-ray emission series is measured, which, to date, consists of emission spectra at a few selected excitation energies (limited by the long acquisition time necessary for reasonable statistics). With the new spectrometer we are now able to measure an emission spectrum for each excitation energy of a regular x-ray absorption scan. Such an x-ray emission "map", typically recorded in 30 minutes, gives unprecedented detailed insight into the electronic structure of solids and liquids.

Isotope and temperature effects in liquid water

Using the above described flow-through liquid cell, we have studied the electronic structure of H_2O and D_2O using XAS and XES (in part discussed in [19]). The experiments were performed at Beamline 8.0 of the ALS. XAS spectra were recorded in total fluorescence yield (TFY) with a channeltron detector, while the XES spectra were measured with the Rowland-circle

spectrograph of the SXF endstation (E/ΔE > 1000 in the present experiments). Resonant x-ray emission maps were recorded with our new x-ray spectrometer described above (E/ΔE>1200). A 100 nm thick Si_3N_4 window membrane (Silson) was used in the liquid cell. Special care was taken to minimize contributions from this membrane to the XAS and XES spectra, including control measurements of oxygen-free liquids and with SiC membranes (NTT Advanced Technologies). In particular, we found that a beam-induced oxidation of the inside surface of the Si_3N_4 membrane can lead to time-dependent and spuriously enhanced XES intensity at 526.7 eV (i.e., at the energy of the low-energy $1b_1$ component discussed below) [24]. In our case, due to special care, spectral contributions related to the membrane were minimized such that they are negligible.

In Fig. 3, XAS spectra of H_2O, D_2O, NaOH, and NaOD are shown. The spectra of H_2O and D_2O consist of two main features: the pre-edge at ~535 eV and the main edge at ~537 eV, which were also observed before [1,2,4]. Note that, due to self-absorption effects, the pre-edge feature is overemphasized as compared to electron yield spectra. The spectra of NaOH and NaOD show the same features, but in addition exhibit a pre-pre-edge resonance at ~533 eV related to the lowest unoccupied molecular orbital (4σ) of OH^-. Comparing the spectra of H_2O with those of D_2O and NaOH with NaOD we find a clear isotope effect. For D_2O and NaOD, a blue-shift of the above described features with respect to the H_2O and NaOH data is observed. While the exact origin of this shift remains to be explained, the fact that no such shift is found in the gas phase absorption spectra of H_2O and D_2O [32] suggests that this effect is correlated to the local hydrogen bonding configuration in the liquid phase. We speculate that the origin of the shift might be due to differences in the hydration shell of H_2O and D_2O. A contribution from zero-point energy is conceivable but can only explain a few ten percent of the shift.

In Fig. 4, the XES spectra of liquid and ice H_2O and D_2O (at non-resonant excitation) and those of NaOH and NaOD (excited at the energy of the pre-pre-edge to avoid contributions from water) are shown. In addition, non-resonant spectra of H_2O at different temperatures are compared. In the following we will describe the various experimental observations and then suggest a model to explain them.

The XES spectra of H_2O and D_2O consist of transitions from three different O 2p-derived molecular orbitals into the O 1s core hole as labeled in Fig. 4 (left), namely $1b_2$, $3a_1$, and $1b_1$ [17,18]. The following observations can be made:

I. Compared to previously published results with inferior energy resolution [9,14], our HRXES spectra of liquid water show a clear splitting of the $1b_1$ orbital. Such a splitting has been observed before for HRXES of ice [18] and is also seen in our spectra of amorphous H_2O and D_2O ice in Fig. 4 (left), but only one peak (the low-energy component) is visible in HRXES spectra of gas phase water [17].

II. There is a strong isotope effect in water. In both, liquid and ice D_2O, the low-energy component of the $1b_1$ emission is significantly weaker than that in the corresponding H_2O spectrum (see Fig. 4, left).

III. Both, the H_2O and the D_2O ice spectra exhibit a stronger low-energy component (relative to the high-energy component) than the spectra of their liquid counterparts (see Fig. 4, left).

IV. A temperature effect can be derived from the H_2O temperature series shown in the bottom spectra of Fig. 4 (left). The inset of Fig. 4 (left) shows a quantification of the decrease of the low-energy $1b_1$ component with increasing temperature.

To analyze the data, we have assumed that the spectra of H_2O and D_2O mainly consist of two distinct components with varying weights. We have then calculated differences of the H_2O and D_2O spectra (with suitable weight factors, as described in [19]), which are shown in Fig. 4 (right). The difference spectrum d_1 (D_2O – 0.62 H_2O) exhibits three emission features similar to the photoemission spectra of water [33], i.e., the $1b_2$, $3a_1$, and the high-energy $1b_1$ component. In contrast, d_2 (H_2O – 0.87 D_2O) only has two features (including the low-energy $1b_1$ component) and is very similar to the emission spectra of NaOH and NaOD, with the exception of a broader tail on the high-energy side of the spectrum.

Observations III and IV suggest that the splitting of the $1b_1$ component can be related to the hydrogen bonding network. Since hydrogen bonds are expected to be more often broken in the liquid state as well as at higher temperatures, the low-energy $1b_1$ component appears to occur preferably for molecules in a highly (i.e., four-fold) coordinated bonding configuration. However, the presence of the strong isotope effect (II) shows that the low-energy $1b_1$ component cannot solely be due to highly coordinated water molecules and the high-energy component to water molecules with distorted hydrogen-bond environment. If that was the case, the isotope effect should be much smaller than the temperature effect and, even more importantly, occur in the opposite direction, since hydrogen bonds are stronger in D_2O.

Based on the above observations and the concept of an excitation-induced dissociation of H_2O and D_2O [12], we have suggested the following model [19]. The emission component d_2 (dominated by the low-energy peak of the $1b_1$ feature) corresponds to dissociated water molecules, namely water molecules that have lost one of their hydrogen (or deuterium) atoms,

whereas the d_1 component corresponds to emission from intact water molecules. This explains the strong isotope effect (II), since the dissociation is expected to be almost twice as fast for H_2O than for D_2O [12]. The spectrum d_2 of the dissociated molecule, as derived by the spectral decomposition described above, should be similar to that of OH, as can be seen in Fig. 4 (right). Assuming that the dissociation of the water molecule is promoted by the presence of hydrogen bonds, in accordance with theoretical results [16,34], both the weak temperature effect (IV) as well as the differences between ice and liquid water (III) can be explained.

Resonant x-ray emission maps of H_2O and D_2O

As mentioned above, our new x-ray spectrometer enables us to measure complete resonant x-ray emission "maps", i.e., a two-dimensional representation of a series of emission spectra for each excitation energy of a regular x-ray absorption scan. Fig. 5 shows the x-ray emission maps of H_2O (left) and D_2O (right). The emission intensity is color-coded and given as a function of emission energy and excitation energy. On the top of each map, the emission spectrum with a (non-resonant) excitation energy of 550 eV is given. On the right-hand side of each map, the integrated intensity of each emission spectrum is displayed, which corresponds to an absorption scan in partial fluorescence yield mode. These spectra are in accordance with the data shown in Figs. 2 and 3.

On the bottom right of the two maps in Fig. 5, we find the Rayleigh (elastically scattered) peak as a diagonal line with equal excitation and emission energies. It exhibits a resonance near the pre-edge absorption onset at 534.5 eV (and a second weak resonance at the main edge at 536.6 eV, not visible on the intensity scale of Fig. 5). We speculate that this resonance is due to an

enhancement of the participant decay channel due to a resonant population of unoccupied molecular states (i.e., $4a_1$ and $2b_2$). Close inspection shows that the first resonance of the Rayleigh line is already observed slightly below the absorption onset, which is attributed to a Coulombic interaction between the excited electron and the oxygen 1s core hole.

On the low emission energy side of the first strong resonance (i.e. below 535 eV), we find additional intensity that extends down to the O K emission spectrum. Just above the first Rayleigh resonance, this additional intensity is particularly strong (indicating the recombination of an electron-hole pair state in the above-described sense). At lower emission energies (between 528.2 and 533.8 eV), the intensity is independent of the emission energy. We attribute this intensity to a continuum of energy losses possible for above-edge excitation in liquid water. We also note that the relative intensity (compared to the main emission region) as well as the exact shape of the losses is different between H_2O and D_2O (and thus the elastic peak near the resonance also has different shape). This can be speculatively explained by the fast dissociation processes described above, leading to different scattering conditions for H_2O and D_2O.

For the main emission region (emission energies of 518 – 529 eV), we observe the following effects. Below the absorption edge, we find a (low) spectral intensity shifting parallel with the excitation energy, i.e., a Raman shift (note that also non-dispersing features are observed, which can be correlated to a non-resonant spectrum excited with higher orders of the beamline). Once the absorption edge is reached, the (resonantly excited) O K emission spectrum emerges. For excitation into the pre-edge, one $1b_1$ component can be observed. Indeed, Hjelte et al. found that, when exciting into the pre-edge, the dominant contribution to resonant Auger spectra of gas phase water stems from dissociated water molecules [35]. Note that the high resolution and

spectral quality of the map approach now allows us to derive unprecedented detail of the resonant spectra. In particular, we find that this component has an emission energy intermediate between the two above-discussed components, and shows significant asymmetry. For the case of H_2O (Fig. 5, left), the main spectral weight is towards lower emission energy, while for D_2O (Fig. 5, right), the main spectral weight is towards higher emission energy. A closer look reveals that for H_2O, a region with low intensity between the two $1b_1$ components exists for all excitation energies. This clearly indicates that the high-energy component (indicative for the undissociated water molecules) does not simply shift towards the low-energy component, but rather decreases strongly with decreasing excitation energy, again in agreement with Hjelte et al. [35] (see above). As expected, the situation is different for D_2O, where the high-energy component still has significant spectral weight at the pre-edge, in agreement with the expected much slower dissociation. In fact, the findings can be summarized such that the spectral weight for pre-edge excitation is transferred towards the dissociated species and that the high-energy component gains in intensity and shifts towards higher emission energies with increasing excitation energy.

For excitation energies above the main edge (i.e., between 538 and 544 eV), we observe a broad resonance in the intensity of the low-energy $1b_1$ component, while the intensity of the high-energy $1b_1$ component remains constant. We note that this energy regime shows high XAS intensity for ice [4] and thus supports our interpretation of enhanced dissociation for highly-coordinated water molecules, which, as discussed above, we associate with the low-energy $1b_1$ component.

Summary

To investigate the electronic structure of water and other liquids using x-ray emission spectroscopy, we have developed a flow-through liquid cell that allows us to control the temperature of the investigated liquid, avoids beam-induced artifacts in the experimental spectra, and enables a fast exchange of liquids. We have measured high-resolution x-ray emission spectra of H_2O and D_2O, revealing a splitting of the $1b_1$ emission that gives insight into the dynamics of liquid water on the time scale of the emission process. We observe a strong isotope effect and can distinguish two different spectral components representing intact and dissociated water molecules, respectively. With the development of a high-resolution, high-throughput soft x-ray spectrometer we are able to measure resonant x-ray emission maps. We have measured such maps for liquid H_2O and D_2O, which give detailed insight into the electronic structure of these liquids, in particular when undergoing resonances in electronic excitation. It is expected that the observed effects will help in the discussion to clarify the geometric and electronic structure of liquid water.

Acknowledgement

We are grateful to the ALS staff, in particular W. L. Yang, for technical support. This work was supported by the German BMBF (projects No. 05 KS4WWA/6 and 05 KS4VHA/4), the Office of Naval Research (M.G.), and the DFG Emmy Noether program (M. Bär). The ALS is supported by the Office of Basic Energy Sciences of the U.S. Department of Energy under Contract No. DE-AC02-05CH11231.

References:

[1] Ph. Wernet, D. Nordlund, U. Bergmann, M. Cavalleri, M. Odelius, H. Ogasawara, L.Å. Näslund, T.K. Hirsch, L. Ojamäe, P. Glatzel, L.G.M. Pettersson, and A. Nilsson, Science **304**, 995 (2004).

[2] J. D. Smith, C.D. Cappa, K.R. Wilson, B.M. Messer, R.C. Cohen, and R.J. Saykally, Science **306**, 851 (2004).

[3] D. Laage and J. T. Hynes, Science **311**, 832 (2006).

[4] S. Myneni, Y. Luo, L.Å. Näslund, M. Cavalleri, L. Ojamäe, H. Ogasawara, A. Pelmenschikov, Ph. Wernet, P. Väterlein, C. Heske, Z. Hussain, L.G.M. Pettersson, and A. Nilsson, J. Phys. Condens. Matter **14**, L213 (2002).

[5] M. Leetmaa, M. Ljungberg, H. Ogasawara, M. Odelius, L.Å. Näslund, and A. Nilsson, J. Chem. Phys. **125**, 244510 (2006).

[6] B. Hetenyi, F. de Angelis, P. Giannozzi, and R. Car, J. Chem. Phys. **120**, 8632 (2004).

[7] L.-Å. Näslund, J. Lüning, Y. Ufuktepe, H. Ogasawara, Ph. Wernet, U. Bergmann, L. G. M. Pettersson, and A. Nilsson, J. Phys. Chem. B **109**, 13835 (2005).

[8] D. Prendergast and G. Galli, Phys. Rev. Lett. **96**, 215502 (2006).

[9] M. Odelius, M. Cavalleri, A. Nilsson, and L.G.M. Pettersson, Phys. Rev. B **73**, 024205 (2006).

[10] R. L. C. Wang, H. J. Kreuzer, and M. Grunze, Phys. Chem. Chem. Phys. **8**, 4744 (2006).

[11] T. Head-Gordon and G. Hura, Chem. Rev. **102**, 2651 (2002).

[12] R. T. Hart, C.J. Benmore, J. Neuefeind, S. Kohara, B. Tomberli, and P.A. Egelstaff, Phys. Rev. Lett. **94**, 047801 (2005).

[13] J.D. Smith, C.D. Cappa, B.M. Messer, W.S. Drisdell, R.C. Cohen, and R.J. Saykally, J. Phys. Chem. B **110**, 20038 (2006).

[14] J.-H. Guo, Y. Luo, A. Augustsson, J.-E. Rubensson, C. Såthe, H. Ågren, H. Siegbahn, and J. Nordgren, Phys. Rev. Lett. **89**, 137402 (2002).

[15] S. Kashtanov, A. Augustsson, Y. Luo, J.-H. Guo, C. Såthe, J.-E. Rubensson, H. Siegbahn, J. Nordgren, and H. Ågren, Phys. Rev. B **69**, 024201 (2004).

[16] M. Odelius, H. Ogasawara, D. Nordlund, O. Fuchs, L. Weinhardt, F. Maier, E. Umbach, C. Heske, Y. Zubavichus, M. Grunze, J.D. Denlinger, L.G.M. Pettersson, and A. Nilsson, Phys. Rev. Lett. **94**, 227401 (2005).

[17] J. Nordgren, L.P. Werme, H. Ågren, C. Nordling, and K. Siegbahn, J. Phys. B: Atom. Molec. Phys. **8**, L18 (1975).

[18] E. Gilberg, M. J. Hanus, and B. Foltz, J. Chem. Phys. **76**, 5093 (1982).

[19] O. Fuchs, M. Zharnikov, L. Weinhardt, M. Blum, M. Weigand, Y. Zubavichus, M. Bär, F. Maier, W. Yang, J. D. Denlinger, C. Heske, M. Grunze, and E. Umbach, Phys. Rev. Lett. 100, 027801 (2008) and Reply to Comment by L.G.M. Pettersson et al., Phys. Rev. Lett., in print.

[20] S. Shin et al., private communication.

[21] L.C. Duda, T. Schmitt, A. Augustsson, and J. Nordgren, J. Alloys Compounds **362,** 116 (2004).

[22] C. Heske, U. Groh, O. Fuchs, L. Weinhardt, E. Umbach, T. Schedel-Niedrig, C.H. Fischer, M.C. Lux-Steiner, S. Zweigart, T.P. Niesen, and F. Karg, J. Chem. Phys. **119** 10467 (2003).

[23] J. Guo, T. Tong, L. Svec, J. Go, C. Dong, and J.-W. Chiou, J. Vac. Sci. Technol. A **25**, 1231 (2007).

[24] O. Fuchs, F. Maier, L. Weinhardt, M. Weigand, M. Blum, M. Zharnikov, J.D. Denlinger, M. Grunze, C. Heske, and E. Umbach, Nuclear Instruments and Methods in Physics Research A **585**, 127 (2008).

[25] O. Fuchs et al., in preparation (Rev. Sci. Instrum.).

[26] M. C. Hettrick and J. H. Underwood, Applied Optics **25** 4228 (1986).

[27] G. Ghiringhelli, A. Piazzalunga, C. Dallera, G. Trezzi, L. Braicovich, T. Schmitt, V.N. Strocov, R. Betemps, L. Patthey, X. Wang, and M. Grioni, Rev. Sci. Instrum. **77**, 113108 (2006).

[28] C.F. Hague, J.H. Underwood, A. Avila, R. Delaunay, H. Ringuenet, M. Marsi, and M. Sacchi, Rev. Sci. Instrum. **76**, 023110 (2005).

[29] T. Hatsui, H. Setoyama, E. Shigemasa, and N. Kosugi, J. Electr. Spectr. Rel. Phenom. **144-147**, 1059 (2005).

[30] T. Tokushima,Y. Harada, H. Ohashi, Y. Senba, and S. Shin, Rev. Sci. Instrum. **77**, 063107 (2006).

[31] J. J. Jia, T. A. Callcott, J. Yurkas, A. W. Ellis, F. J. Himpsel, M. G. Samant, J. Stöhr, D. L. Ederer, J. A. Carlisle, E. A. Hudson, L. J. Terminello, D. K. Shuh, and R. C. C. Perera, Rev. Sci. Instrum. **66** (1995), 1394-1397.

[32] A. Hiraya, K. Nobusada, M. Simon, K. Okada, T. Tokushima, Y. Senba, H. Yoshida, K. Kamimori, H. Okumura, Y. Shimizu, A.-L. Thomas, P. Millie, I. Koyano, and K. Ueda, Phys. Rev. A **63**, 042705 (2001).

[33] B. Winter, R. Weber, W. Widdra, M. Dittmar, M. Faubel, and I.V. Hertel, J. Phys. Chem. A **108**, 2625 (2004).

[34] B. Brena, D. Nordlund, M. Odelius, H. Ogasawara, A. Nilsson, and L.G.M. Pettersson, Phys. Rev. Lett. **93**, 148302 (2004).

[35] I. Hjelte, M.N. Piancastelli, R.F. Fink, O. Björneholm, M. Bässler, R. Feifel, A. Giertz, H. Wang, K. Wiesner, A. Ausmees, C. Miron, S. L. Sorensen, and S. Svensson, Chem. Phys. Lett. **334**, 151 (2001).

Figure captions:

FIG. 1. Sketch of the flow-through liquid cell (from [24]).

FIG. 2. Sketch of the optical path of the spectrometer. The Aperture "A" can be used to mask the spherical mirror "M". "G" denotes a blazed VLS grating, and "D" a back-illuminated CCD detector in normal incidence geometry (from [25]).

FIG. 3. O K-edge XAS spectra of liquid H_2O/D_2O and NaOH/NaOD solutions, acquired at T = 277 K (from [19]).

FIG. 4. Left, from top to bottom: non-resonant ($h\nu$ = 550.1 eV) XES spectra of amorphous H_2O and D_2O ice, of liquid H_2O and D_2O, and of H_2O at different temperatures. Right, from top to bottom: non-resonant spectra of H_2O and D_2O, differences between these two spectra (d_1: D_2O-0.62 H_2O, d_2: H_2O-0.87 D_2O), and resonant spectra of NaOH/NaOD solutions ($h\nu$ = 533.5 eV). The spectra of the liquids were acquired at T = 277 K, those of ice at T ~ 100 K (modified from [19]).

FIG. 5. Resonant x-ray emission maps of H_2O (left) and D_2O (right). The emission intensity is color-coded and given as a function of emission energy and excitation energy. The upper panel shows a non-resonant x-ray emission spectrum (excitation energy: 550 eV). The right panel shows an absorption spectrum with fluorescence yield detection, i.e., the integrated O K emission intensity as a function of excitation energy.

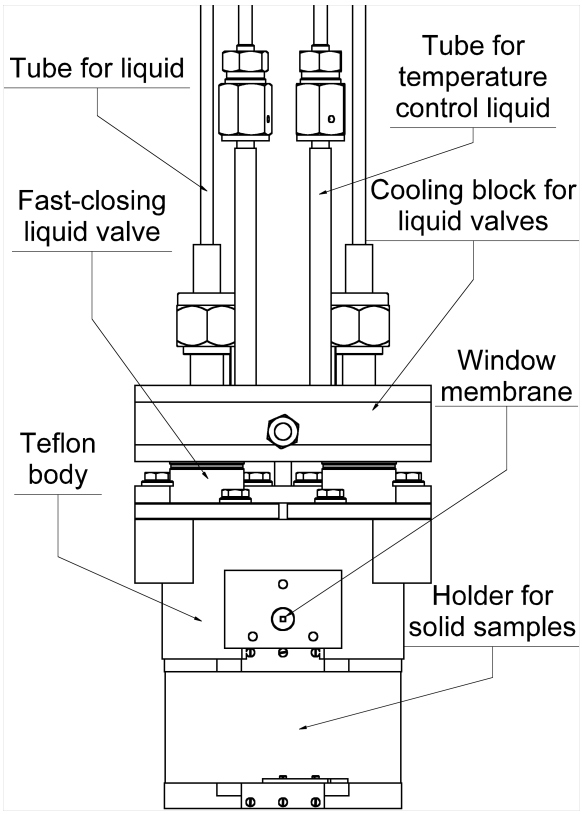
Tube for liquid
Tube for temperature control liquid
Fast-closing liquid valve
Cooling block for liquid valves
Window membrane
Teflon body
Holder for solid samples

Figure 1

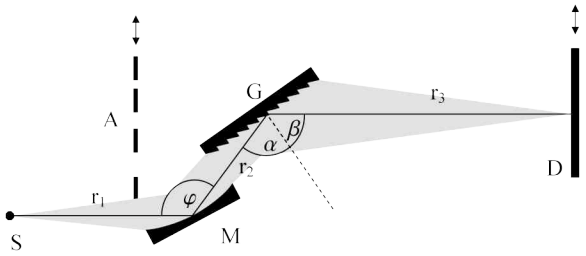

Figure 2

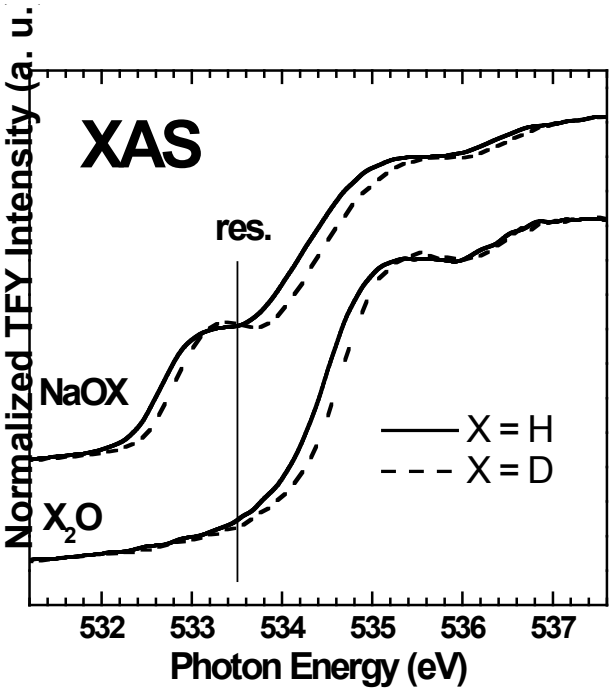
XAS
res.
NaOX
X2O
X = H
X = D
Normalized TFY Intensity (a. u.)
532
533
534
535
536
537
Photon Energy (eV)

Figure 3

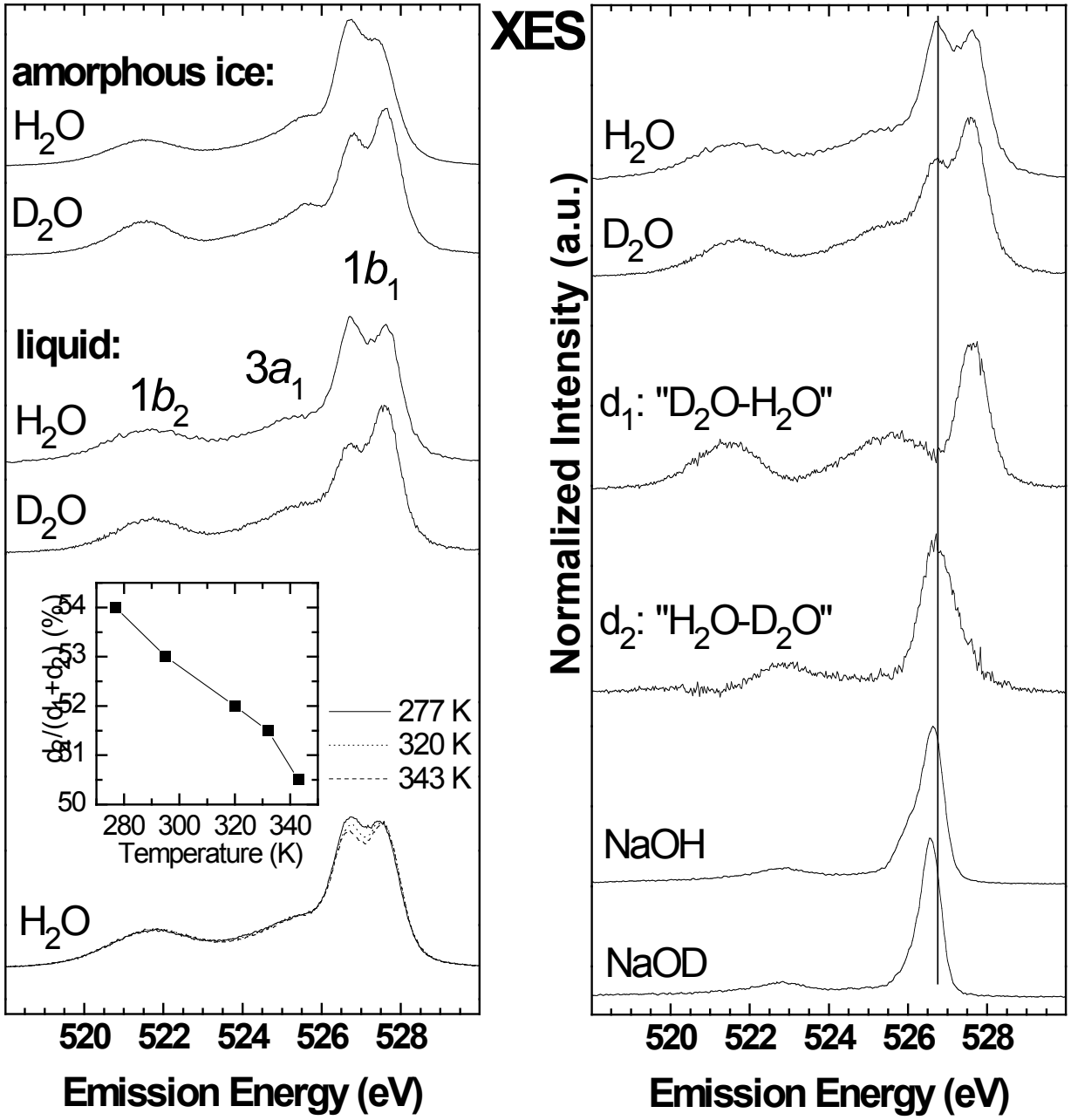
XES
amorphous ice:
H2O
D2O
1b1
liquid:
3a1
1b2
H2O
D2O
d1/(d1+d2) (%)
277 K
320 K
343 K
Temperature (K)
H2O
520 522 524 526 528
Emission Energy (eV)
Normalized Intensity (a.u.)
H2O
D2O
d1: "D2O-H2O"
d2: "H2O-D2O"
NaOH
NaOD
520 522 524 526 528
Emission Energy (eV)

Figure 4

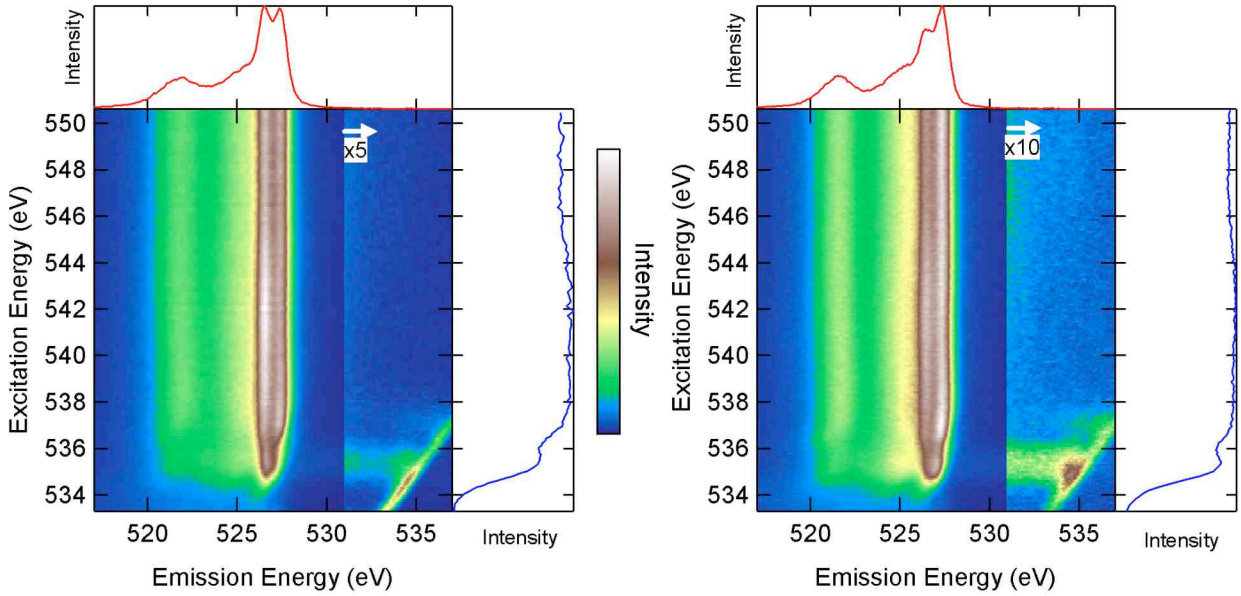
Intensity
Excitation Energy (eV)
550
548
546
544
542
540
538
536
534
x5
520
525
530
535
Emission Energy (eV)
Intensity
Intensity
Intensity
Excitation Energy (eV)
x10
Emission Energy (eV)
Intensity

Figure 5